

# Growth and helicity of non-centrosymmetric $\text{Cu}_2\text{OSeO}_3$ crystals

Aisha Ageel, Jan Sahliger, Guowei Li, Jacob Baas, Graeme R. Blake, Thomas. T.M. Palstra and Christian H. Back

Dr. A. Ageel, J. Sahliger

Physik-Department, Technische Universität München, D-85748 Garching, Germany

Dr. G. Li

Max Planck Institute for Chemical Physics of Solids, 01187 Dresden, Germany

ing. J. Baas, Dr. G. R. Blake, Prof. Dr. Thomas. T.M. Palstra <sup>1</sup>

Zernike Institute for Advanced Materials, University of Groningen, Nijenborgh 4, 9747 AG Groningen, The Netherlands

<sup>1</sup> Present address: University of Twente, 7522NB Enschede, The Netherlands

Prof. Dr. C. H. Back

Physik-Department, Technische Universität München, D-85748 Garching, Germany

Munich Center for Quantum Science and Technology (MCQST), D-80799 München, Germany

Email Address: christian.back@tum.de

Keywords: *Chiral magnet, chemical vapor transport,  $\text{Cu}_2\text{OSeO}_3$ , X-ray diffraction, single crystals, non-centrosymmetric magnets*

We have grown  $\text{Cu}_2\text{OSeO}_3$  single crystals with an optimized chemical vapor transport technique by using  $\text{SeCl}_4$  as a transport agent. Our optimized growth method allows to selectively produce large high quality single crystals. The method is shown to consistently produce  $\text{Cu}_2\text{OSeO}_3$  crystals of maximum size 8 mm x 7 mm x 4 mm with a transport duration of around three weeks. We found this method, with  $\text{SeCl}_4$  as transport agent, more efficient and simple compared to the commonly used growth techniques reported in literature with  $\text{HCl}$  gas as transport agent. The  $\text{Cu}_2\text{OSeO}_3$  crystals have very high quality and the absolute structure are fully determined by simple single crystal x-ray diffraction. We observed both type of crystals with left- and right-handed chiralities. Our magnetization and ferromagnetic resonance data show the same magnetic phase diagram as reported earlier [1].

## 1 Introduction

Investigation of complex magnetic systems is generally limited by an inability to obtain sufficiently large, pure high quality crystals. This is especially true for the noncentrosymmetric magnets with chirality. In this class of materials the interactions that may lead to symmetry breaking magnetic order do not cancel each other when evaluated over the unit cell. The most well studied chiral systems are  $\text{MnSi}$  [2, 3],  $\text{Mn}_{1-x}\text{Fe}_x\text{Ge}$  [4],  $\text{FeGe}$  [5] and semiconducting  $\text{Fe}_{1-x}\text{Co}_x\text{Si}$  [6]. In these chiral magnets, the principal magnetic phases are a helical phase, a single domain conical phase and a skyrmion state (known as A-phase). They appear in a small magnetic field-temperature (B-T) pocket close to transition temperature  $T_c$ . In the chiral atomic framework of this crystal family, the orbital motions of localized electrons also take helical paths. The neighbouring spins of localized electrons are coupled by the relativistic spin-orbit interaction called Dzyaloshinskii-Moriya (DM) interaction [7, 8]. As the sign of the DM interaction is determined by the chemical composition, it emphasizes that the magnetic chirality is intrinsically dependent on the lattice handedness. It has been shown experimentally in  $\text{Mn}_{1-x}\text{Fe}_x\text{Ge}$  crystals that the skyrmion helicity is directly determined by the crystal helicity [4].

$\text{Cu}_2\text{OSeO}_3$  is one of the most important members of the chiral group with the  $\text{P}2_13$  chiral cubic crystal structure. It is the first insulator in which the skyrmion lattice has been observed [9, 10] with a very similar B-T phase diagram as the other related members of this chiral group. Recently, some new magnetic phases like tilted conical spiral [11], low-temperature skyrmion lattice phase [12] and elongated skyrmions [13] have been observed in  $\text{Cu}_2\text{OSeO}_3$ . The insulating behavior of this magnetic material makes the study of the decisive role of crystal helicity especially more interesting by excluding other contributions due to conduction electrons. To understand the unique magnetic structure of  $\text{Cu}_2\text{OSeO}_3$ , several different techniques have been employed including,  $\mu\text{-SR}$  [14], Lorentz transmission electron microscopy [10], ac-susceptibility measurements [15], Terahertz Electron Spin Resonance [16], time-resolved

magneto-optics [17]. Recently, generation of spin currents have been studied in  $\text{Cu}_2\text{OSeO}_3$  by spin pumping experiments [18].

Considering the large interest in the magnetic properties of  $\text{Cu}_2\text{OSeO}_3$ , it is important to look for new, efficient and fast single crystal growth techniques. Conventionally,  $\text{Cu}_2\text{OSeO}_3$  crystals are grown by vapor transport method with HCl gas as transport agent. With this growth method only one helicity has been reported [19]. The other helicity has not been reported to the best of our knowledge. It is known that the structural and magnetic chiralities for  $\text{Cu}_2\text{OSeO}_3$  crystals are directly related with each other [19]. Therefore to use both magnetic chiralities, it is needed to improve the growth techniques not only to speed up the growth rate but also to get crystals with both chiralities. Here, we report a new and fast way for the growth of  $\text{Cu}_2\text{OSeO}_3$  single crystals with  $\text{SeCl}_4$  as transport agent. We observed very high quality crystal growth yielding both chiralities with this new growth technique. The crystal structure of  $\text{Cu}_2\text{OSeO}_3$  crystals has been studied before [20, 21, 22] with different diffraction techniques. Here, we used the simplex single crystal x-ray diffraction (XRD) to establish the absolute structures for both handedness, which also emphasizes good quality of the crystals.

## 2 Experimental

Single crystals of  $\text{Cu}_2\text{OSeO}_3$  were grown by the standard chemical-vapor transport method. However, the novelty of this growth is the use of selenium tetrachloride ( $\text{SeCl}_4$ ) as a transport agent. Previously,  $\text{SeCl}_4$  is mainly used to grow the molybdenum and tungsten diselenides. In literature  $\text{Cu}_2\text{OSeO}_3$  is usually grown by HCl gas [23], here, we report the growth of chiral magnets with  $\text{SeCl}_4$  as transport agent which is new and different from literature [24]. For growth, transparent quartz ampoules (30 mm inside diameter, 30 cm length) were used. They were first carefully cleaned with ethanol, acetone, 10% HF and demi water and dried overnight at 200 °C before the charge was introduced.  $\text{SeCl}_4$  is very hygroscopic; therefore, it was weighed and introduced into the transport tubes in a glove box under a nitrogen atmosphere. Mixtures of high-purity CuO (Alfa-Aldrich, 99.995 %) and  $\text{SeO}_2$  (Alfa-Aldrich, 99.999%) powders in a molar ratio of 2:1 were sealed in an evacuated quartz ampoule with 0.54 g of  $\text{SeCl}_4$  (Alfa-Aldrich, 99.5%). After a few minutes of degassing, the part of the ampoule containing the chemicals was immersed into liquid nitrogen, subsequently evacuated and sealed after the chemicals had cooled below evaporation temperatures. The ampoule was then placed horizontally into a tubular three-zone furnace having 18 cm - long zones separated by a distance of 3 cm. The temperature of the furnace was raised gradually by 50 °C/h to 600 °C. To get rid of unwanted nucleation centers, a reverse temperature gradient was applied by adjusting the temperature of the source zone ( $T_{\text{hot}}$ ) to 610 °C and the deposition zone ( $T_{\text{cold}}$ ) to 660 °C for 24h. Afterwards,  $T_{\text{hot}}$  and  $T_{\text{cold}}$  were adjusted to 610 °C and 570 °C, respectively, for growth. These furnaces were regulated by a PID electronic regulator (SHINKO) with  $\pm 0.5$  °C temperature stability at 500-650 °C. After two weeks, shiny crystals could be seen at the deposition zone. After four weeks, the ampoules were quenched at the source zone so that all gas vapours would quickly condense at the source zone. The extreme hygroscopic nature of  $\text{SeCl}_4$  resulted in the presence

Table 1: Growth conditions for  $\text{Cu}_2\text{OSeO}_3$  with CVT growth method for different transport agents (TA).

TA	$T_{\text{hot}}$ (°C)	$T_{\text{cold}}$ (°C)	duration of growth (d)	max. size of crystals ( $\text{mm}^3$ )
HCl [23]	620	580	49	130-150
$\text{SeCl}_4$	610	570	23	210-224

of water in the ampoules, in spite of all precautions taken. The presence of water can create the vapor phase of hydrogen chloride (HCl) and a chalcogen oxichloride ( $\text{SeOCl}$ ), thus making the analysis of the transport mechanism more complex. However, we observed that the presence of moisture slows down the transport process. This transport method with  $\text{SeCl}_4$  resulted in reasonably big and thick crystals. To compare the efficiency of the growth method, we also synthesized the crystals with HCl gas as transport agent as reported in literature [23]. The growth conditions are summarized in Table 1. The crystal structure of  $\text{Cu}_2\text{OSeO}_3$  crystals is investigated by D8 Venture single crystal x-ray diffraction (XRD).

The crystal quality is checked with precision scans of XRD for full sphere approximation. The morphology and elemental analysis were examined using a Philips XL 30 scanning electron microscopy (SEM) equipped with a EDS system, which was operated at an accelerating voltage of 20 kV. The magnetization measurements were done using a Quantum Design MPMS-XL 7 SQUID magnetometer.

To further study the phase magnetic phase diagram of  $\text{Cu}_2\text{OSeO}_3$ , we performed ferromagnetic resonance (FMR) measurements using a broadband spin-wave spectroscopy technique [25, 13] on both HCl and  $\text{SeCl}_4$  grown crystals. For this purpose we used two polished crystals with similar dimensions: HCl grown sample with size -  $1.5 \times 2.5 \times 0.5 \text{ mm}^3$  and  $\text{SeCl}_4$  grown crystal with size -  $2.9 \times 2.7 \times 1 \text{ mm}^3$ . The crystals were polished using the technique reported in Ref. [26]. The coplanar waveguides with a signal line of  $50 \mu\text{m}$  width and gap of  $25 \mu\text{m}$  width were patterned. The CPWs were directly patterned onto the oriented polished crystals with (110) and (111) surface, respectively. They were patterned by e-beam lithography followed by e-beam evaporation of Ti (10nm)/Au (150nm). The excitation field distribution of the CPWs is shown in Fig. 4(b). The samples with CPW were mounted on a continuous flow cryostat. A vector network analyzer (VNA) was used to measure the resonance signals. The temperature reading of the cryostat was different from the MPMS system used to measure the magnetization data due to the placement of the temperature sensor. The temperature difference (7K -10K) between both setups is adjusted in the manuscript. A rotatable electromagnet was used to provide the static magnetic field up to 500 mT.

### 3 Results

A tiny single crystal grown with  $\text{SeCl}_4$  was selected for morphology and element analysis as shown in Figure 1(a). The as synthesized crystal has a rough surface with many tiny nanoparticles attached on it. The molar ratio of Se, Cu, and O are determined to be very close to the stoichiometric  $\text{Cu}_2\text{OSeO}_3$  sample. Furthermore, the energy dispersive spectrometer(EDS) elemental mapping (Figure 1(b)-(d)) demonstrates that the Cu, O, and Se atoms are uniformly distributed, which unambiguously reveals the uniformity of the single crystal. That is, a homogeneous and high-quality sample was successfully synthesized with such a simple method. Table 2 shows the parameters used to establish the absolute structure of  $\text{Cu}_2\text{OSeO}_3$  single crystals.  $\text{Cu}_2\text{OSeO}_3$  crystals display the  $P2_13$  space group and the ions occupy the Wyckoff positions that are summarised in Table 3. The precision scans of XRD for full sphere approximation shows the high quality of  $\text{Cu}_2\text{OSeO}_3$  single crystals without any twinning.

Table 2: Crystallographic data and structure refinement for  $\text{Cu}_2\text{OSeO}_3$  single crystals.

Temperature	100 K
crystal system	cubic
space group	$P2_13$
wave length	$0.7107 \text{ \AA}^\circ$
unit cell dimension a	$8.9446 \text{ \AA}^\circ$
$\theta$ range for data collection	$3.147^\circ - 32.25^\circ$
Limiting indices	$-13 \leq h \leq 13$ $-11 \leq k \leq 11$ $-13 \leq l \leq 13$
Reflections collected / unique	0.0367
Final R indices [ $I > 2\sigma(I)$ ]	0.0312
Absolute structure parameter	-0.01(2)

The chirality of the crystals has been characterized by the Flack parameter analysis. The Flack parameter is defined as the ratio between two opposite-handed domains for non-centrosymmetric crystals giving rise to a resonant contribution in the x-ray scattering amplitudes. A Flack parameter equal to zero corresponds to a single domain of the chiral structure (enantiopure) and a Flack parameter equal to 1 represents a single domain structure but with opposite chiralities. The absolute structures are solved by calculating the atomic coordinates during refinement of the Flack parameter x by using the twin model

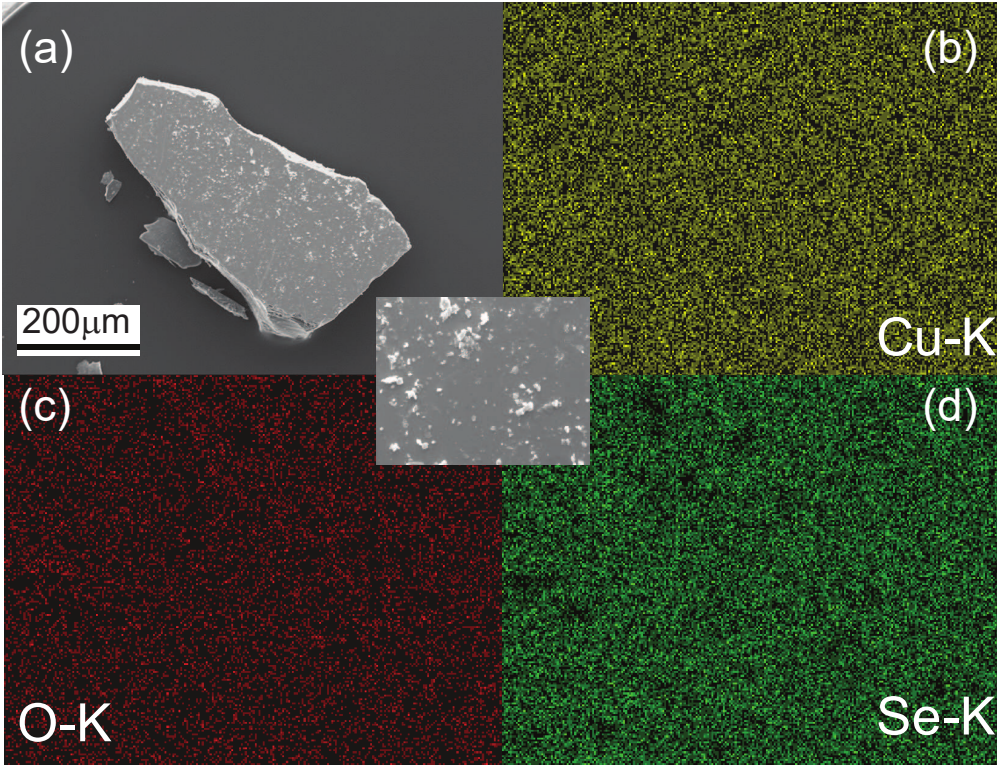


Figure 1: (a) The SEM image of a typical single crystal. EDS elemental mapping for Cu (b), O (c), and Se (d) elements in the as synthesized crystal. The inset show the scanning area for element mapping.

for intensities of hkl reflections as follows:

$$I_{hkl}^{calc} = (1-x) |F_{hkl}|^2 + x |F_{-h-k-l}|^2 \quad (1)$$

Here,  $|F_{hkl}|$  and  $|F_{-h-k-l}|$  represent the structure factors. The dual-space SHELXL method was used for the structure determination. The full sphere of Bragg reflections was used for refinement. Results of least square refinement gives a Flack x of 0.013(17) indicating two absolute structures having opposite chirality. The deviation factor is defined as:

$$R_1 = \Sigma |F_{obs} - F_{calc}| / \Sigma F_{obs} \quad (2)$$

The standard deviation  $R_1$  was found to be 0.0217, which shows that the scattering strictly follows the Flack conditions. We measured eight crystals to resolve the absolute structure, in which we found five right-handed and three left-handed enantiomers. The atomic coordinates for absolute structures for left-handed and right-handed enantiomers of  $Cu_2OSeO_3$  are summarized in Table 3.

Table 3: Atomic coordinates and Wyckoff positions (WF) for  $Cu_2OSeO_3$  for both handedness.

	WP	Right-handed			Left handed		
		x	y	z	x	y	z
Cu (1)	4a	0.88589(3)	0.88589(3)	0.88589(3)	0.11404(4)	0.11404(4)	0.11404(4)
Cu (2)	12b	0.13439(3)	0.12108(3)	0.87247(3)	0.86549(4)	0.87895(4)	0.12754(4)
Se (1)	4a	0.45963(3)	0.45963(3)	0.45963(3)	0.54031(4)	0.54031(4)	0.54031(4)
Se (2)	4a	0.21201(3)	0.21201(3)	0.21201(3)	0.78802(4)	0.78802(4)	0.78802(4)
O (1)	4a	0.01031(3)	0.01031(3)	0.01031(3)	0.98974(3)	0.98974(4)	0.98974(3)
O (2)	12b	0.76232(2)	0.76232(2)	0.76232(2)	0.23730(3)	0.23730(4)	0.23730(3)
O (3)	4a	0.27029(2)	0.48318(2)	0.46954(2)	0.72971(3)	0.51663(4)	0.53014(3)
O (4)	12b	0.27257(2)	0.18681(2)	0.03276(2)	0.72786(3)	0.81329(4)	0.96738(3)

Figure 3(a) shows the temperature dependence of field-cooled magnetization measurements under an applied field  $H$  varying from 100 Oe to 1500 Oe with a  $T_c \approx 60$  K.

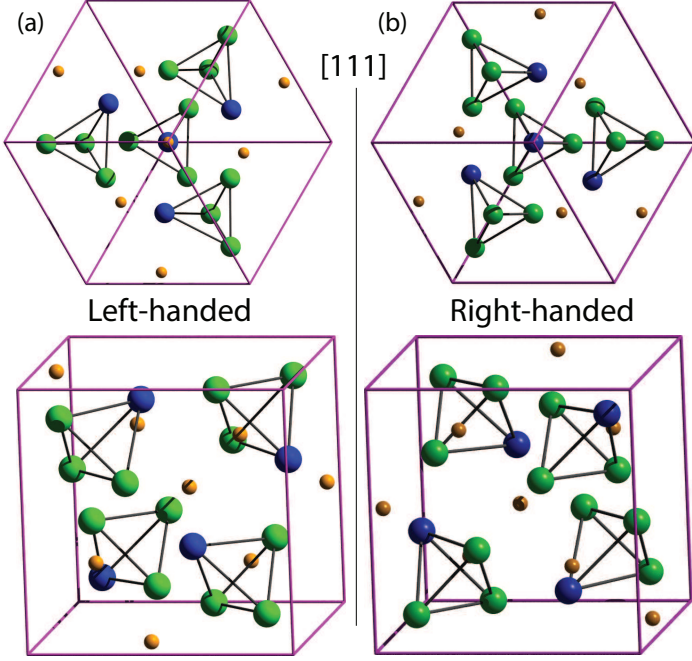


Figure 2: The two chiral crystal structures of  $\text{Cu}_2\text{OSeO}_3$  where green and blue spheres represent  $\text{Cu1}$  and  $\text{Cu2}$  atoms. The top views are along the body diagonal of the cube (along  $[111]$  axis). (a) right-handed and (b) left-handed crystals.

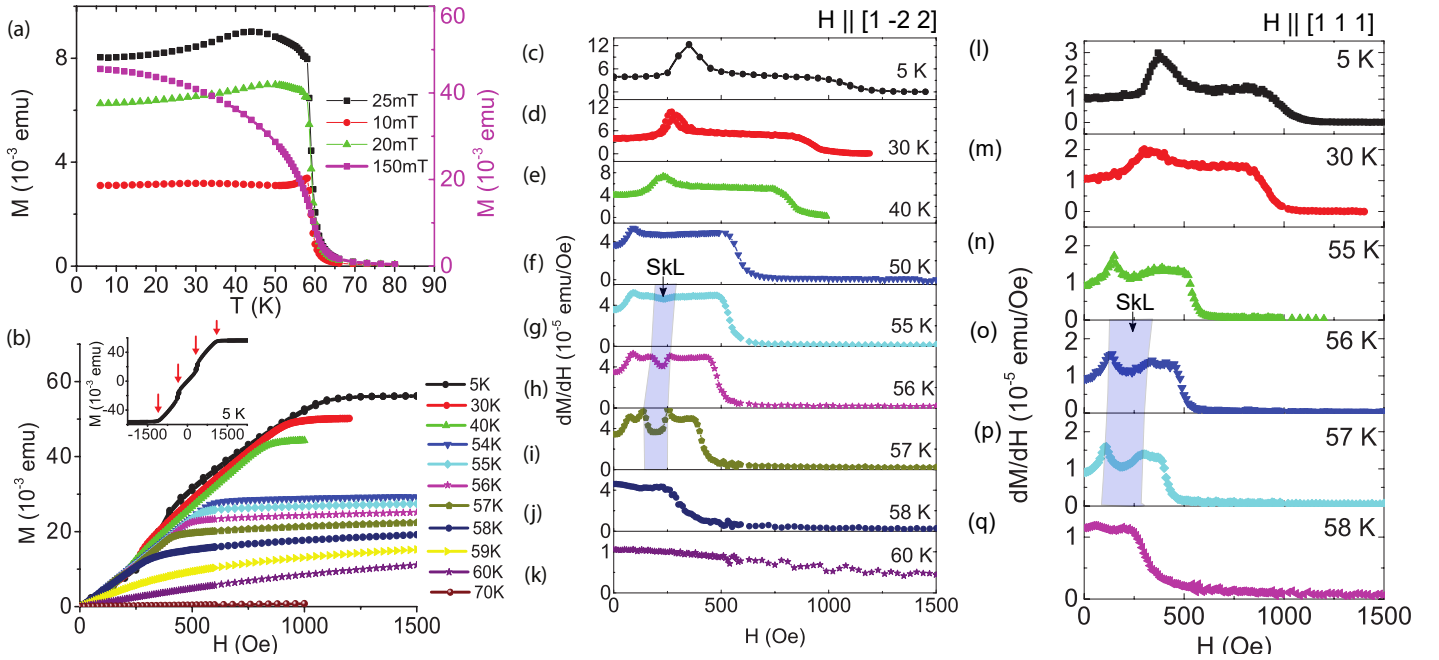


Figure 3: (a) Temperature dependences of the FC magnetic susceptibilities in different applied magnetic fields along  $[001]$  direction. (b) Magnetic field dependence of the magnetization at different temperatures, with magnetic field applied along  $[1-22]$  direction. The inset shows the slope-change behavior at the fields  $\sim 350$  Oe and  $1100$  Oe at 5 K, as indicated by arrows. The  $dM/dH$  vs  $H$  at different temperatures with magnetic field applied along (c)-(k)  $[1-22]$  and (l-q)  $[111]$  crystallographic directions. The shaded region represents the skyrmion lattice phase.



The FMR spectra were measured as reported earlier [13] and the background free transmission signal was defined as  $|\Delta S_{21}|^2 = (|S_{21}(H) - |S_{21}(H_0)|)^2$ .  $S_{21}(H)$  and  $S_{21}(H_0)$  are the complex transmissions measured with VNA at a fixed magnetic field  $H$  and  $H_0$ , respectively. An example of such spectra measured for HCl and  $\text{SeCl}_4$  grown samples are shown in Figs. 4(d) and 4(e), respectively. These spectra are used to construct the high temperature magnetic phase diagram of  $\text{Cu}_2\text{OSeO}_3$  shown in Fig 4(f).

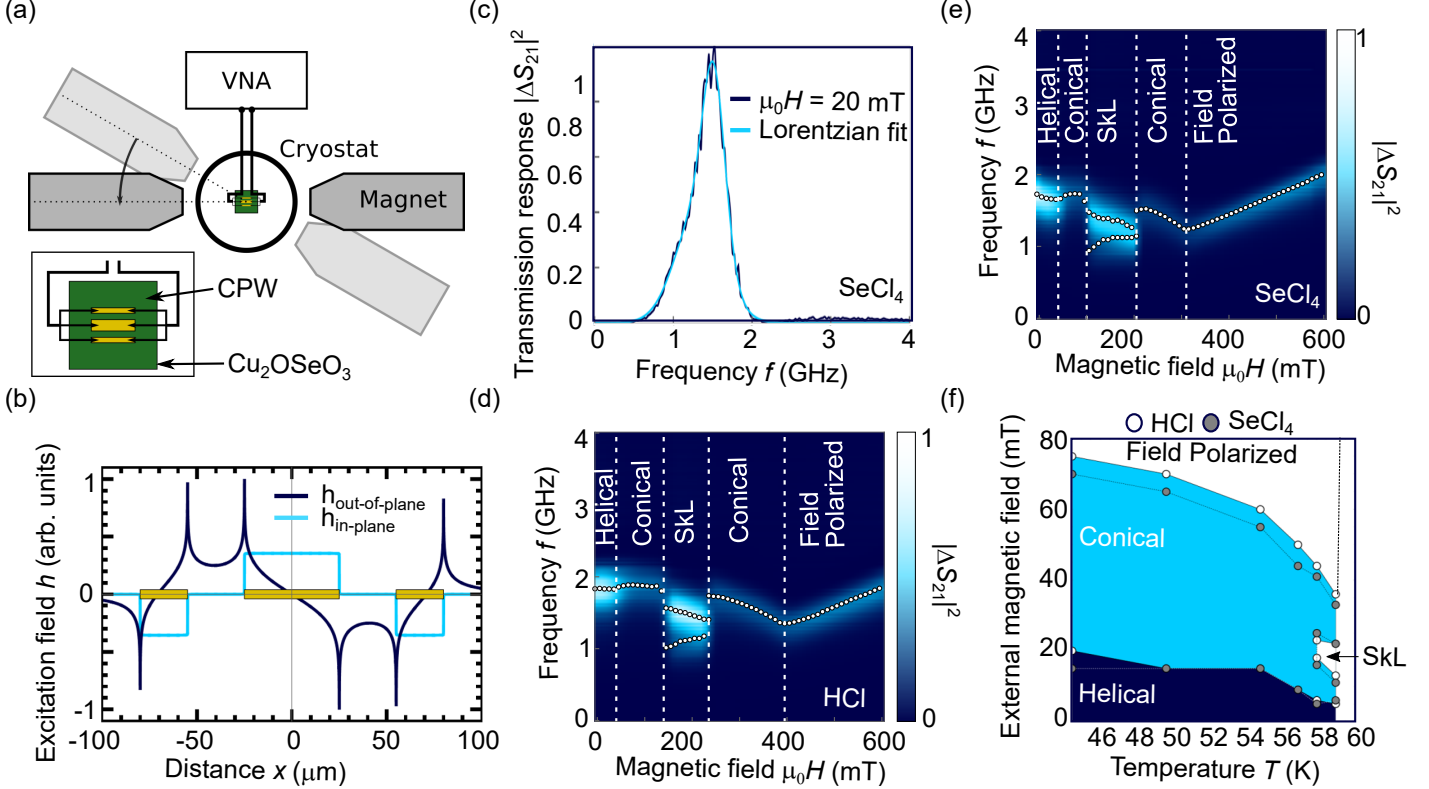


Figure 4: Schematics of the broad band ferromagnetic resonance setup with a vector network analyzer (VNA), low temperature measurement setup (cryostat) and a rotatable electromagnet. The inset shows the schematics of the coplanar waveguide (CPW) structured directly onto the sample surface. The static magnetic field  $H$  is applied along the CPW within the plane of the sample along the  $[1-11]$  crystallographic direction of  $\text{Cu}_2\text{OSeO}_3$ . (b) Field distribution of the CPW. (c) Transmission difference  $\Delta|S_{21}|^2$  as a function of frequency measured at 20mT at 5 K. (d-e) Color-coded resonance map obtained from the line scans of the transmission response measured as a function of frequency at 58 K for the HCl and  $\text{SeCl}_4$  grown samples. (f) The magnetic phase diagram of  $\text{Cu}_2\text{OSeO}_3$  single crystals obtained by applying static magnetic field along  $[1-11]$  crystallographic direction of  $\text{Cu}_2\text{OSeO}_3$ . The phase boundaries (dots) are extracted from the resonance spectra shown in 4(d,e).

## 4 Discussion

The vapor transport technique [23] commonly used for the growth of  $\text{Cu}_2\text{OSeO}_3$  single crystals is relatively slow and complex due to use of the HCl gas as transport agent. However, the method reported in this paper is very simple and easy due to use of solid transport agent  $\text{SeCl}_4$  and also found to be relatively fast. A disadvantage of  $\text{SeCl}_4$  transport agent could be the strong silica attack and its strong hygroscopic nature which can be easily settled by using the transport agent in an inert and dry atmosphere.  $\text{SeCl}_4$  is frequently used in the past as an efficient transport agent for the growth of diselenides as  $\text{WSe}_2$  and  $\text{MoSe}_2$  [27, 24, 28]. Like  $\text{SeCl}_4$ ,  $\text{TeCl}_4$  can also be an efficient transport agent.  $\text{TeCl}_4$  is more stable and less hygroscopic compared to  $\text{SeCl}_4$  which makes it more suitable transport agent compared to  $\text{SeCl}_4$  for vapor transport growth. However,  $\text{TeCl}_4$  can dope the crystals and therefore,  $\text{SeCl}_4$  is more suitable for growth of un-doped  $\text{Cu}_2\text{OSeO}_3$  crystals. The decomposition of  $\text{SeCl}_4$  will give a mixture of Selenium and dichlorine that can result in possible gaseous oxygen compounds during transport for  $\text{SeCl}_4$  can be  $\text{SeO}_2$ ,  $\text{SeOCl}_2$  and  $\text{SeO}$ . Chlorine resulting from the decomposition of  $\text{SeCl}_4$  is probably playing

the efficient role in the transport but the role of the Selenium is not very clear in the transport. In case of presence of water, the transport would be more complicated by also involving HCl vapors for the transport. We observed a clear decrease in the deposition rate by exposing the  $\text{SeCl}_4$  transport agent to the air.

The absolute structures were solved for six different crystals, grown with  $\text{SeCl}_4$  as transport agent. During refinement the Goodness of Fit (GooF) was found to be 0.9-1.03 and the scale factor K is 0.95-1.0 and the standard deviation R1 is found to be 0.2-0.5, which confirms the high quality of these crystals. Four out of six analyzed crystals showed the same helicity and the other two crystals showed the opposite. The helicity can be defined from the Wyckoff position of magnetic ions. In the case of  $\text{Cu}_2\text{OSeO}_3$ , Cu(1) and Cu(2) ions are located at 4a and 12b Wyckoff position as shown in Table 3. The 4a Wyckoff position of Cu(1) in  $\text{Cu}_2\text{OSeO}_3$  is  $(x, x, x/0.5+x, 0.5-x, -x/-x, 0.5+x, 0.5-x/0.5-x, -x, 0.5+x)$  where  $x \approx 0.136$  or  $x \approx 1 - 0.136 = 0.863$  corresponding to two enantiomers. The crystals having Cu(1) at  $x = 0.863$  are defined as right-handed enantiomer and others with  $x = 0.136$  as left-handed enantiomer as shown in Table 3. The structure of  $\text{Cu}_2\text{OSeO}_3$  with the same set of coordinates for the right-handed crystals shown in Table 3 is also defined as right-handed in Ref. [19]. There, the crystals are defined as right-handed on the basis of similarity of 4a Wyckoff position of Cu(1) ion in  $\text{Cu}_2\text{OSeO}_3$  and Mn in MnSi (right-handed).

The crystal helicity can also be defined by considering the closeness of the structural symmetry of the  $\text{P2}_13$  space group with the absolute structure of  $\text{P4}_132$  as proposed by Ref. [29].  $\text{P4}_132$  space group contains only right-handed screw axes  $4_1$ , therefore the right-handed crystals of  $\text{P2}_13$  space group can be easily distinguished by comparison. The same approach is also mentioned for B20 structures [30]. The set of coordinates determined with this definition for right-handed crystals is found to be consistent with the obtained absolute structure for the right-handed crystals as shown in Table 3.

The magnetization and resonance data shown in Figs. 3 and 4 show the presence of the skyrmion lattice phase along with other magnetic phases of  $\text{Cu}_2\text{OSeO}_3$ . To determine the linewidths and peak positions from the transmission signal, Lorentzian peak fitting was used. An example of such peak fitting is shown in Fig 4(c). The resonance spectra measured for both samples grown with HCl and  $\text{SeCl}_4$  qualitatively show no clear difference (cf. Figs. 4(d) and 4(e)). For both samples, resonance signal with similar linewidth is observed, confirming that the crystals grown with the new method have the same damping as for those grown with the HCl [31]. The phase boundaries of the skyrmion lattice for both samples grown with HCl and  $\text{SeCl}_4$  coincide with each other (see 4(f)).

## 5 Conclusion

We have demonstrated a simple route that allows the growth of  $\text{Cu}_2\text{OSeO}_3$  single crystals in a relatively short duration. The XRD analysis shows high quality of single crystals. We observed both right-handed and left-handed enantiomers of  $\text{Cu}_2\text{OSeO}_3$  and the absolute structure was fully determined by the Flack parameter analysis of the refined XRD pattern. The growth of crystals with both left- and right-handed structural chiralities can be useful to understand the coupling between structural and magnetic chiralities. The understanding of the coupling is important to control the magnetic textures such as skyrmions for spintronics applications.

## Acknowledgements

We thank H. Berger, T. Nilges and N. Tombros for fruitful discussions. F. Reiter for assistance with the experiments. This work has been funded by the Deutsche Forschungsgemeinschaft (DFG, German Research Foundation) under TRR80 (From Electronic Correlations to Functionality, Project No. 107745057, Project G9) and the excellence cluster MCQST under Germany's Excellence Strategy EXC-2111 (Project No. 390814868).

## References

- [1] F. Qian, H. Wilhelm, A. Aqeel, T. T. M. Palstra, A. J. E. Lefering, E. H. Brück, C. Pappas, *Phys. Rev. B* **2016**, *94* 064418.
- [2] S. Mühlbauer, B. Binz, F. Jonietz, C. Pfleiderer, A. Rosch, A. Neubauer, R. Georgii, P. Böni, *Science* **2009**, *323*, 5916 915.
- [3] F. Jonietz, S. Mühlbauer, C. Pfleiderer, A. Neubauer, W. Münzer, A. Bauer, T. Adams, R. Georgii, P. Böni, R. A. Duine, K. Everschor, M. Garst, A. Rosch, *Science* **2010**, *330*, 6011 1648.
- [4] S. K., X. Z. Yu, T. Hara, D. Morikawa, N. Kanazawa, *Nature Nanotechnology* **2013-10**, *8*, 10 723.
- [5] X. Z. Yu, N. Kanazawa, Y. Onose, K. Kimoto, W. Z. Zhang, S. Ishiwata, Y. Matsui, Y. Tokura, *Nature Materials* **2011-2**, *10*, 2 106.
- [6] W. Münzer, A. Neubauer, T. Adams, S. Mühlbauer, C. Franz, F. Jonietz, R. Georgii, P. Böni, B. Pedersen, M. Schmidt, A. Rosch, C. Pfleiderer, *Phys. Rev. B* **2010**, *81* 041203.
- [7] I. Dzyaloshinsky, *Journal of Physics and Chemistry of Solids* **1958**, *4*, 4 241 .
- [8] T. Moriya, *Phys. Rev.* **1960**, *120* 91.
- [9] T. Adams, A. Chacon, M. Wagner, A. Bauer, G. Brandl, B. Pedersen, H. Berger, P. Lemmens, C. Pfleiderer, *Phys. Rev. Lett.* **2012**, *108* 237204.
- [10] S. Seki, X. Z. Yu, S. Ishiwata, Y. Tokura, *Science* **2012**, *336*, 6078 198.
- [11] F. Qian, L. J. Bannenber, H. Wilhelm, G. Chaboussant, L. M. Debeer-Schmitt, M. P. Schmidt, A. Aqeel, T. T. M. Palstra, E. Brück, A. J. E. Lefering, C. Pappas, M. Mostovoy, A. O. Leonov, *Science Advances* **2018**, *4*, 9.
- [12] A. Chacon, L. Heinen, M. Halder, A. Bauer, W. Simeth, S. Mühlbauer, H. Berger, M. Garst, A. Rosch, C. Pfleiderer, *Nature Physics* **2018**, *14*, 9 936.
- [13] A. Aqeel, J. Sahliger, T. Taniguchi, S. Mändl, D. Mettus, H. Berger, A. Bauer, M. Garst, C. Pfleiderer, C. H. Back, *Phys. Rev. Lett.* **2021**, *126* 017202.
- [14] A. Maisuradze, Z. Guguchia, B. Graneli, H. M. Rønnow, H. Berger, H. Keller, *Phys. Rev. B* **2011**, *84* 064433.
- [15] I. Levatić, V. Šurija, H. Berger, I. Živković, *Phys. Rev. B* **2014**, *90* 224412.
- [16] M. Ozerov, J. Romhányi, M. Belesi, H. Berger, J.-P. Ansermet, J. van den Brink, J. Wosnitza, S. A. Zvyagin, I. Rousochatzakis, *Phys. Rev. Lett.* **2014**, *113* 157205.
- [17] N. Ogawa, S. Seki, Y. Tokura, *Sci. Rep.* **2015**, *5*.
- [18] D. Hirobe, Y. Shiomi, Y. Shimada, J.-i. Ohe, E. Saitoh, *Journal of Applied Physics* **2015**, *117*, 5 053904.
- [19] V. Dyadkin, K. Prša, S. V. Grigoriev, J. S. White, P. Huang, H. M. Rønnow, A. Magrez, C. D. Dewhurst, D. Chernyshov, *Phys. Rev. B* **2014**, *89* 140409.
- [20] G. Meunier, M. Bertaud, *Journal of Applied Crystallography* **1976**, *9*, 4 364.
- [21] H. Effenberger, F. Pertlik, *Monatshefte für Chemie / Chemical Monthly* **1986**, *117*, 8-9 887.
- [22] J.-W. G. Bos, C. V. Colin, T. T. M. Palstra, *Phys. Rev. B* **2008**, *78* 094416.
- [23] M. Belesi, I. Rousochatzakis, H. C. Wu, H. Berger, I. V. Shvets, F. Mila, J. P. Ansermet, *Phys. Rev. B* **2010**, *82* 094422.



- [24] J. Legma, G. Vacquier, A. Casalot, *Journal of Crystal Growth* **1993**, *130*, 1–2 253 .
- [25] T. Schwarze, J. Waizner, M. Garst, A. Bauer, I. Stasinopoulos, H. Berger, C. Pfleiderer, D. Grundler, *Nature Materials* **2015**, *14*, 5 478.
- [26] A. Aqeel, I. J. Vera-Marun, B. J. van Wees, T. T. M. Palstra, *Journal of Applied Physics* **2014**, *116*, 15 153705.
- [27] A. Klein, Y. Tamm, R. Schlaf, C. Pettenkofer, W. Jaegermann, M. Lux-Steiner, E. Bucher, *Solar Energy Materials and Solar Cells* **1998**, *51*, 2 181 .
- [28] G. Prasad, O. N. Srivastava, *Journal of Physics D: Applied Physics* **1988**, *21*, 6 1028.
- [29] V. Chizhikov, V. Dmitrienko, *J. Magnetism and Magnetic Materials* **2015**, *382*, 0 142 .
- [30] V. Dmitriev, D. Chernyshov, S. Grigoriev, V. Dyadkin, *J. Phys.: Condens. Matter* **2012**, *24*, 36 366005.
- [31] I. Stasinopoulos, S. Weichselbaumer, A. Bauer, J. Waizner, H. Berger, S. Maendl, M. Garst, C. Pfleiderer, D. Grundler, *Applied Physics Letters* **2017**, *111*, 3 032408.